GEOMETRY OF PHASE-SEPARATED DOMAINS IN PHOSPHOLIPID BILAYERS BY DIFFRACTION-CONTRAST ELECTRON MICROSCOPY

S. W. HUI, *Electron Optics Laboratory, Biophysics Department, Roswell Park Memorial Institute, Buffalo, New York 14263*

ABSTRACT The sizes and shapes of solidus (gel) phase domains in the hydrated molecular bilayers of dilauroylphosphatidylcholine/dipalmitoylphasphatidylcholine (DLPC/DPPC) (1:1) and phosphatidylserine (PS)/DPPC (1:2) are visualized directly by low dose diffraction-contrast electron microscopy. The temperature and humidity of the bilayers are controlled by an environmental chamber set in an electron microscope. The contrast between crystalline domains is enhanced by electron optical filtering of the diffraction patterns of the bilayers. The domains are seen as a patchwork in the plane of the bilayer, with an average width of 0.2–0.5 μm. The percentage of solidus area measured from diffraction-contrast micrographs at various temperatures agrees in general with those depicted by known phase diagrams. The shape and size of the domains resemble those seen by freeze-fracture in multilamellar vesicles. Temperature-related changes in domain size and in phase boundary per unit area are more pronounced in the less miscible DLPC/DPPC mixture. No significant change in these geometric parameters with temperature is found in the PS/DPPC mixture. Mapping domains by their molecular diffraction signals not only verifies the existance of areas of different molecular packing during phase separation but also provides a quantitative measurement of structural boundaries and defects in lipid bilayers.

INTRODUCTION

The phase transition of lipid bilayers and the lateral phase separation in bilayers of mixed phospholipids have been known to affect the structure and function of certain biomembranes (1–5). Studies of the phase behavior of phospholipid bilayers (6) suggest that during phase change, both fluidus (liquid crystalline) and solidus (gel) areas coexist. The ratio of molecules in the fluidus and solidus phases may be deduced from the phase diagram. However, for a given ratio of fluidus to solidus molecules, the relative amount of lipid molecules in the "phase boundary" and in the "bulk" may vary depending on the shape and the average size of individual phase-separated areas (domains). Structural mismatch is expected along the phase boundary. It has been suggested that the geometry of structural mismatching, rather than the bulk fluidity, affects the thermal hystersis (7), annealing (8), permeability (9–11), protein-lipid interaction (12, 13) and susceptibility to enzymes (14) of bilayers. It may also be a factor in membrane flow (15, 16) and fusion (8, 17, 18). Lipid microdomain structures have been related to the capping of surface immunogloblin in lymphocytes (19). There has been some discussion about the size of cooperative units during phase transition in a single-component system (9, 20–22). Recently a computer modeling of the lateral distribution of molecules in two-component lipid bilayers has been reported (23). However, no direct experimental

measurement of domain size and boundary length in multicomponent phospholipid bilayers is available.

In this paper, the technique of diffraction-contrast electron microscopy is used to record directly the geometry of phase-separated domains of different molecular packings. The term geometry here means the measurements of the size, shape, and distribution of domains. This method is based on optical filtering at the diffraction plane in the microscope to distinguish images of crystallites of different molecular packings and orientations. The diffraction-contrast technique is often used in metallurgy to map different grains in thin films of alloys. In the experiments presented here, bilayers of various hydrated phospholipid mixtures were placed in an environmental stage set in an electron microscope. The size and shape of phase-separated domains in the bilayer were photographed at various temperature ranges. The image data thus obtained provide not only the molar ratio of lipids in each bulk phase at given temperature but also the geometry of domains and their boundaries. This information cannot be deduced from calorimetry and x-ray diffraction measurements. A preliminary account of this technique has been published (24).

Two phospholipid mixtures, phosphatidylserine/dipalmitoylphosphatidylcholine (PS/DPPC)[1] at molar ratio (1:2) and dilauroylphosphatidylcholine (DLPC)/DPPC at molar ratio (1:1), are used in this study. These two mixtures have similar phase-transition ranges but different miscibilities. Differing by four carbons in length, DLPC and DPPC are only partially miscible (25). The transition temperature of the 1:1 mixture spans 0° and 35°C, with the lower and upper endothermic peaks at 5° and 30°C in the differential scanning thermogram (26). The bovine brain PS used in the PS/DPPC mixture contains mostly oleic and linoleic acid residues, has a broad transition at 0°–10°C, and is miscible with DPPC. The 1:2 mixture has a broad transition from 20°–40°C, peaking at 35°C (27). Their physicochemical properties are expected to affect their domain geometry. The purpose of this study is to demonstrate that micrometer-size domains of different molecular packing exist in these lipid mixtures, and that the geometry of these domains depends on the physicochemical properties of the lipids.

MATERIALS AND METHODS

Lipids

L-α-DPPC, L-α-DLPC, and PS from bovine brain were kindly provided by Dr. D. Papahadjopoulos (previously at this Institute). These phospholipids were purified and synthesized by methods previously described (10). Purity of the lipids was checked by thin-layer chromatography. The lipids, 1 mM in chloroform solutions, were sealed in nitrogen-filled ampules and stored at −70°C until use.

Bilayer Formation and Environmental Control

The lipids were mixed under nitrogen to a given molar ratio. The mixture was spread with a microliter pipette onto the vapor/liquid interface of a teflon Langmuir trough to form a monolayer. The trough was maintained at 4°C. The vapor phase was water-vapor–saturated nitrogen, and the liquid phase was a buffer solution containing 100 mM NaCl, 5 mM *N*-Tris-(hydroxymethyl)-methyl-2-aminoethane

[1] *Abbreviations used in this paper:* DMPC, dimyristoylphosphatidylcholine; DPPC, dipalmitoylphosphatidylcholine; DLPC, dilauroylphosphatidylcholine; PS, phosphatidylserine; TES, *N*-Tris-(hydroxymethyl)-methyl-2-aminoethane sulfonic acid.

sulfonic acid (TES), 5 mM histidine, at pH 7.4. The spread monolayers were compressed to a surface pressure of 40 dyne/cm (28). Unsupported bilayers were formed over the holes of 1,000-mesh electron microscope grids by a single dipping method as described (29). This method usually results in a single bilayer and not multilayers (see Results). These unsupported single bilayers were stable in saturated water vapor. The grids were loaded into the specimen holder under water-saturated nitrogen and transferred to the environmental stage, which had been filled with saturated water vapor and precooled to 5°C. The environmental stage used in this experiment has been described elsewhere (30). The stage was installed in a Siemens 1A Elmiskop. (Siemens Corp., Cherry Hill, N. J.) The specimen was placed in the inner chamber of the stage, which was connected to a water reservoir, so that the specimen was maintained at saturated water vapor pressure at all controlled temperatures. The vapor saturation in the chamber was frequently checked by the diffraction of catalase crystals, which are irreversibly destroyed if the vapor pressure drops below 94% of the saturation value.

Electron Microscopy and Diffraction

Electron diffraction patterns of each specimen were recorded at various temperatures as described (29). Special filters made to select different spacings or different orientations of the diffraction pattern were inserted through the objective aperture holder to selectively block out certain parts of the pattern. Two kinds of selective filters were used. One consisted of an annulus of 250-μm mean Diam with an annular gap opening of 20 μm. The mean diameter of the annulus at the back focal plane of the objective lens corresponded to the 4.2-Å diffraction ring for a 100-kV incident electron beam. The annular filter selected only the diffracted beam produced by the solidus state of the lipid chain packing; the 4.7-Å diffuse diffraction produced by the fluidus state of the lipid chain packing was excluded. The other filter consisted of six 100-μm Diam holes, evenly spaced on a 300-μm Diam circle. The inner arcs of these holes selected only the diffraction patterns from those solidus domains so orientated that their hexagonal diffraction patterns were aligned with the orientation of these six holes, and excluded diffraction from solidus domains of other orientations, as well as that from fluidus domains. Because the unscattered beam was also blocked by these filters, the images produced by the selected diffraction beams were dark-field images. In these dark-field micrographs, the domains whose reflections passed through the filters appeared bright. In the experiment, the objective lens was initially focused for a magnification setting of 4,000. The intermediate lens was then focused on the back focal plane of the objective lens, thus projecting the diffraction pattern on the viewing screen. A filter was inserted and positioned so that the diffraction ring or arcs from solidus domains were visible through the opening of the filter. The intermediate lens was then quickly switched to a preset current to focus on the first image plane, thus projecting the dark-field image to be photographed. To minimize radiation damage to the specimen, focusing was carried out on an area adjacent to the area photographed. In some cases, conventional, nonselective dark-field images produced by the tilted-beam technique were also taken, to distinguish the mass-thickness effect from the diffraction effect.

The procedure for freeze-fracture preparation has been described (27). Multilamellar vesicles of given compositions were equilibrated either in 30% glycerol or between thin copper "sandwiches" in an environmental chamber attached to a quick-freeze apparatus (31) and freeze-quenched at given temperatures. Freeze-fracture was performed in a Polaron E7500 unit (Polaron Instruments, Inc., Doylestown, Pa.); electron micrographs were taken in a Siemens 101 electron microscope.

Radiation Damage Assessment

Precaution was taken to ensure that the incident beam dose needed to record electron images of the lipid molecules was below the damaging threshold (32–34), which in this study was determined by alterations of the (01) reflection used for diffraction-contrast imaging. To assess the threshold dosage for each sample at each given temperature, a series of consecutive, short exposure diffraction patterns were recorded at given time intervals while the same sample area was continuously exposed to the incident electron beam. Control exposures were taken at the same time intervals, but the beam was deflected away from the test area in between exposures. Changes in both the diffraction intensity and pattern orientation as functions of time and cumulative radiation were measured by a micro-densitometer

(Joyce-Loebl and Co., Ltd., Gateshead-on-Tyne, England). The incident electron beam was limited by maximally energizing the first condenser lens and by using a 30-μm second condenser aperture. The incident beam on the specimen was limited to an area 5–10 μm in Diam. Under typical experimental conditions, the electron beam current density at the specimen level was 0.5–1 $\times$ 10^{-5} A/cm^2. Images and diffraction patterns were recorded on Kodak No Screen x-ray film (Eastman Kodack Co., Rochester, N. Y.) for high sensitivity. The exposure time was usually 5 s. The total beam dose to the specimen per exposure never exceeded 5 $\times$ 10^{-5} coulomb/cm^2, or one-fourth of the lowest threshold dose. The beam current was measured by an electrometer (Keithley 600, Keithley Instruments, Inc., Cleveland, Ohio) connected to an insulated screen, the collection efficiency of which was calibrated by a Faraday cage.

Geometric Measurement

The diffraction-contrast micrographs recorded at 4,000$\times$ were photographically enlarged to a total magnification of 12,000$\times$. The domain boundaries were traced manually. In order to differentiate mass-thickness effects due to sample unevenness and occasional water condensation on the bilayer, tracings were in some cases determined by comparing prints on different contrast grade papers, and by comparing diffraction-contrast micrographs with conventional dark-field micrographs. The total length of the domain boundary and the total selected domain areas per unit sample area were traced on the pressure-sensitive graphic digitizer pad and computed in the attached calculator (model 241, Ladd Research Industries Inc., Burlington, Vt.). For each data point in Figs. 3 and 4, statistics were obtained by surveying a total sample area 250 to 500 μm^2, except in freeze-fracture micrographs, where a total area of 75 μm^2 was surveyed for each data point. Only the relatively flat surface portions of large vesicles were sampled in the freeze-fracture micrographs.

RESULTS

Diffraction-Intensity Measurements

Because of the mosaic spread (35), the solidus diffraction pattern from an area of 100 μm^2 of hydrated phospholipid bilayer consists of overlapping, hexagonally arranged arcs (Fig. 1), rather than spots (29). Usually only the (01) reflections at 4.2 Å were recorded above the noise level of the film in these low-dose exposures (10^{-5} coulomb/cm^2). The alterations of the (01) reflection intensity and pattern orientation were recorded as functions of cumulative damage by the incident electron beam (Fig. 1). The change of total diffraction intensity as a

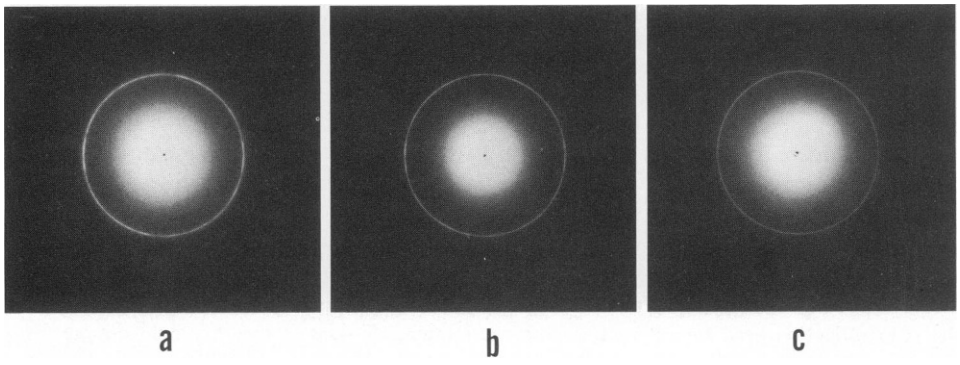

FIGURE 1. Sequence of diffraction patterns from an area of 150 μm^2 of PS/DPPC (1:2) bilayer at 18°C showing the effect of radiation damage. The mean cumulative radiation doses are (*a*) 2 $\times$ 10^{-5}, (*b*) 2.8 $\times$ 10^{-4}, (*c*) 1.04 $\times$ 10^{-3} coulomb/cm^2 at the specimen level. The exposures were taken with 4 $\times$ 10^{-5} coulomb/cm^2 each. (1 coulomb/cm^2 = 625 e/Å^2.)

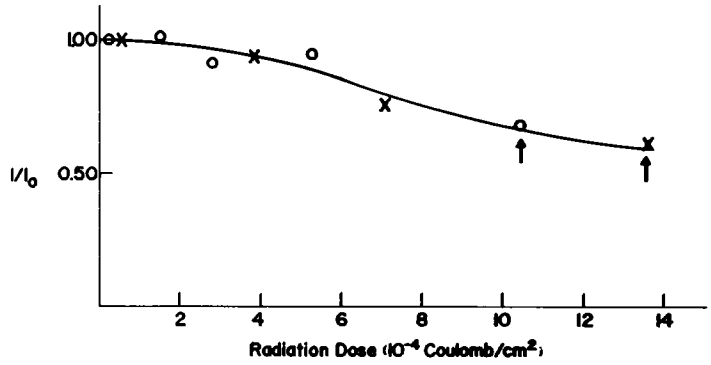

FIGURE 2 Integral diffraction intensity of the (01) reflections of hydrated PS/DPPC (1:2) bilayers (O), and of DLPC/DPPC (1:1) bilayers (×) at 18°C, as functions of cumulative electron radiation. The points marked by arrows are taken just before the rupture of the bilayer.

result of radiation damage is shown in Fig. 2. Insignificant changes were observed from a control exposure series on an adjacent area over the same duration. The measurement was repeated at each experimental temperature. The radiation dose that induced a change in diffraction intensity above the observation error (3%) was designated to be the damage threshold. Both this threshold dose and the dose required to rupture the unsupported bilayer were temperature dependent. At all experimental temperatures, the threshold stayed $>2 \times 10^{-4}$ coulomb/cm^2, whereas the rupture dose was $\sim 10^{-3}$ coulombs/cm^2. A detailed account of the radiation damage study will be given elsewhere.

The total scattering power of the unsupported specimen film was measured as the intensity ratio of the unscattered beam before and after the rupture of the film. Because the total scattering is determined by the mass thickness of the specimen, the thickness of the film may be estimated from the intensity ratio, if the density of the specimen is given. Let the density of lipid and water be 1.0 and the scattering cross section per unit mass be 3.5×10^4 cm^2/g (36). A mean ratio of 0.97 showed the thickness of the membrane to be between 50 and 100 Å. This thickness agreed with that of a single bilayer. We rigorously calculated the theoretical scattering power of a bilayer (29) by using the atomic scattering factors for carbon, hydrogen, and phosphorous (35), by assuming an average area per molecule to be between 40 and 65 Å^2 (28, 37) with an average chain length of 16 carbons, and by integrating the total angular scattering intensity up to 5-m radian. The result of this calculation supported the thickness estimate, which indicated that the film was a single bilayer rather than a multilayer. As a further check, the total scattering power of unsupported multilayer films was measured for comparison. The multilayer films were formed by dipping a grid through a surface layer, which was forced to collapse under excess surface pressure (38). An average intensity ratio of 0.83 showed the films to have about eight bilayers.

Domain-Geometry Measurements

DLPC-DPPC AT MOLAR RATIO (1:1) At least two diffraction-contrast electron micrographs were taken at a given temperature in each of the three repeated experiments. In each experiment, the temperature of the specimen was raised from 5° to 45°C, then lowered to 5°C. Micrographs were taken at 2°C intervals after the specimen had equilibrated at the

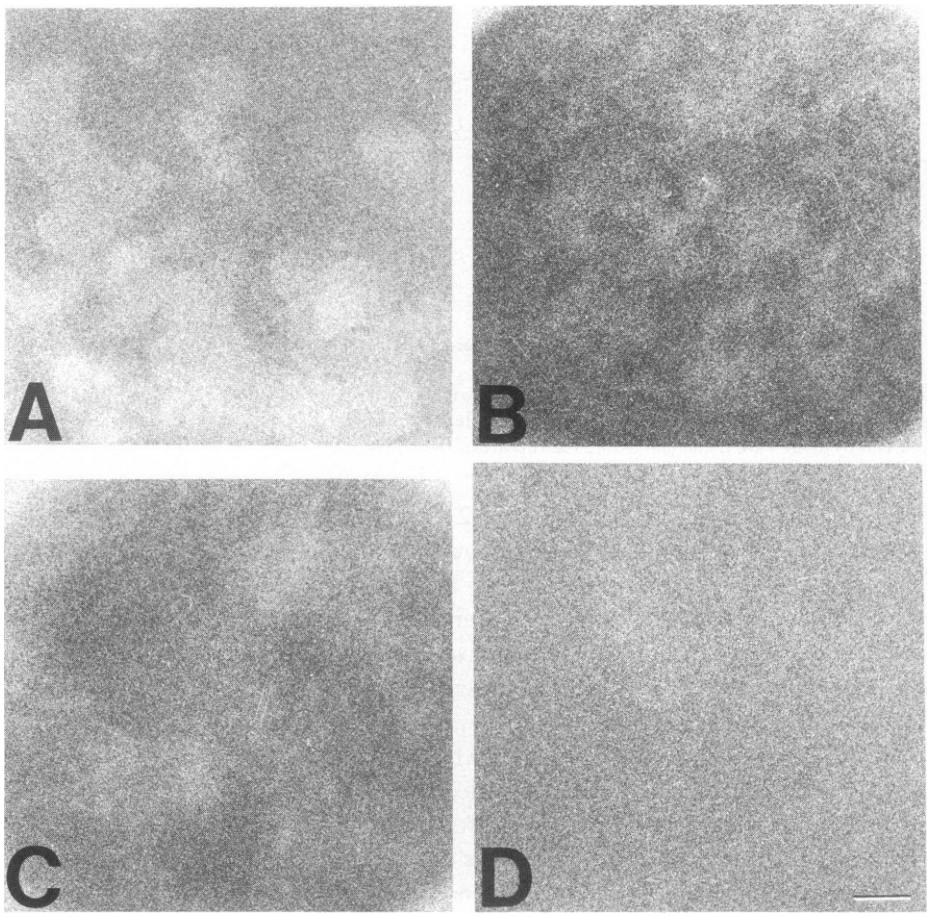

FIGURE 3 Diffraction-contrast micrographs of DLPC/DPPC (1:1) showing solidus domains (white area) at (*A*) 0°C, (*B*) 10°C, (*C*) 20°C, and (*D*) 40°C. Bar, 1 μm.

desired temperature for 3 min. The heating-cooling rate and the equilibrating time was slower than that in most calorimetry experiments. Four micrographs are presented in Fig. 3. The contrast patterns shown in the micrographs did not appear in conventional dark-field micrographs of the same area. The contrast patterns were therefore attributed specifically to the filtered (01) reflections rather than to the nonspecific scattering from areas of different mass-thickness. The domains appeared to have a "patchwork" arrangement. Each domain was 0.1–0.5 μm wide, being wider at lower temperatures.

The sum of the selectively exposed areas (white areas in Fig. 3) was measured as a percentage of the total area of the micrographs. The six-hole filter used for diffraction-contrast imaging had an opening of 55%. On the average, even when all domains were solidus, only 55% of the image area was selected by the filter. The percentage of exposed area in the micrographs must be normalized by 1/0.55 to obtain the true percentage of solidus area. Thus, some normalized experimental values might appear to be >100%, counting experimental error. Results obtained during the heating and cooling cycles differed little, apart from an

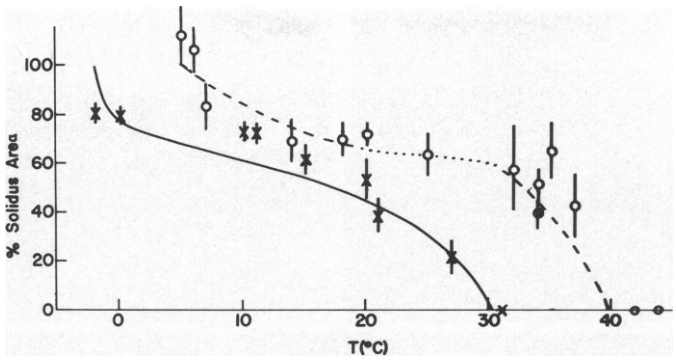

FIGURE 4 Normalized percentage area of solidus domain, at various temperatures in DLPS/DPPC (1:1) bilayer (×), and in PS/DPPC (1:2) bilayer (○) measured from diffraction-contrast micrographs and in PS/DPPC (1:2) (●), measured from freeze-fracture micrographs. The solid and dashed lines are measured from ratios of tie lines drawn on the phase diagrams of DLPC/DPPC (25) and PS/DPPC (27), respectively.

apparent temperature hysteresis of 3°C near the higher onset temperatures. The normalized area percentages are shown in Fig. 4 as a function of temperature. At the higher end of the temperature scale, the contrast of the images was reduced, due partly to the innate movement of the domains (39), and resulted in additional measurement error. The solid line was deduced from the ratio of tie lines of the 1:1 molar mixture, using the phase diagram based on calorimetric results (25). The molar ratio was converted to area ratio using the reported average area per molecule for each phase (37). At temperatures >35°, there were no observable 4.2-Å diffraction rings, and the diffraction-contrast micrographs were featureless, indicating that all observed area was in the liquidus phase.

The periphery or boundary length per unit area was measured as a function of temperature. This parameter reflects the size and shape of the selected domains. Error in these measurements was caused mainly by the uncertainty of mapping the low-contrast domains. The periphery length per unit area was found to increase with temperature (Fig. 5). The solid line

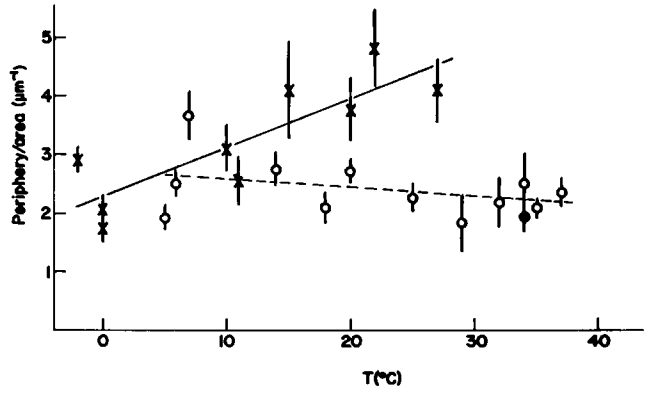

FIGURE 5 Periphery length per unit area of selected solidus domain as functions of temperature. The symbols are given in the caption of Fig. 4. The solid and dashed lines are results of linear regression. Error bars include variations between micrographs as well as uncertainty in domain tracing.

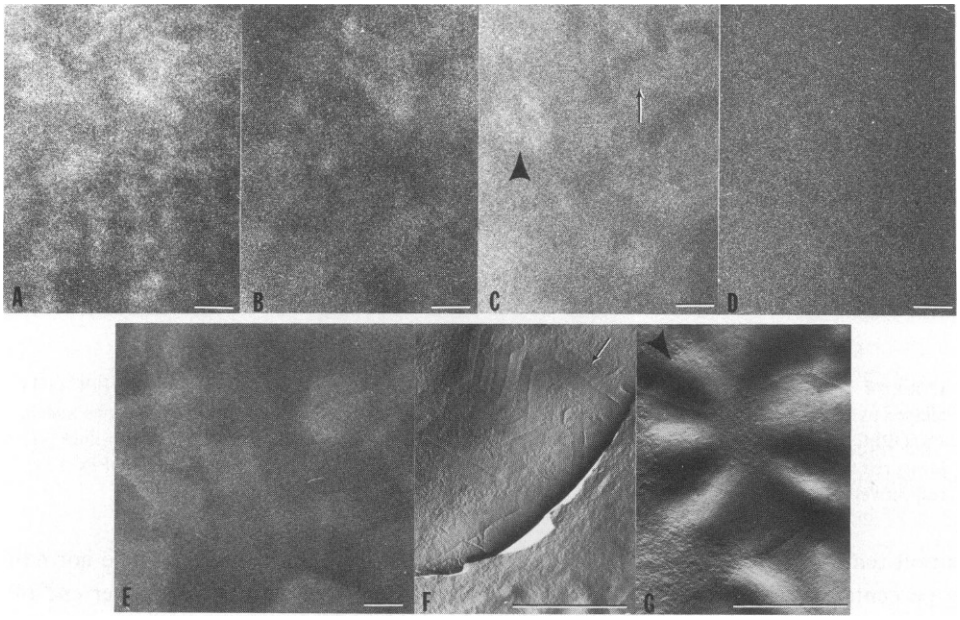

FIGURE 6 Diffraction-contrast micrographs of PS/DPPC (1:2) showing solidus domains (white area) at (*A*) 5°C, (*B*) 20°C, (*C*) 35°C, (*D*) 44°C, and of PS/DPPC (1:10) at (*E*) 5°C. Freeze-fracture micrographs of multilamellar vesicles of PS/DPPC (1:2) quenched at 34°C (*F*, *G*) are shown for comparison. Arrows point to solidus domains of similar shapes in diffraction contrast (*C*) and freeze-fracture (*F*, *G*) micrographs. The thick arrows point to "rings" while the thin arrows point to straight-edged "stripes." Bars, 1 μm.

is the linear regression line. This trend indicated that the domains became smaller and narrower as temperature was increased, in agreement with visual examination results. (Fig. 3).

PS-DPPC AT MOLAR RATIO (1:2) Diffraction-contrast electron micrographs (Fig. 6) were again obtained from three repeated experiments. A plot of the normalized percentage of solidus area as a function of temperature is presented in Fig. 4. The dashed curve is the percentage of solidus area derived from tie lines drawn in the phase diagram of Stewart et al. (27). Because of the uncertainty of the $P_{\beta'} - L_{\beta'}$ phase transition in the phase diagram, tie lines in the 18°–30°C temperature range could not be accurately drawn. At temperatures between 30° and 40°C, percentage of solidus domain could also be measured from freeze-fracture micrographs by using the characteristic banded pattern of the solidus phase, which was very distinguishable from the smooth or jumbled fracture face of the fluidus phase. The area percentage thus measured is also shown in Fig. 4 (solid circle). The size of the solidus domains seen in diffraction-contrast micrographs (white areas in Fig. 6*C*) is comparable to that seen in freeze-fracture micrographs of samples quenched at the same temperatures (banded areas in Fig. 6*F*, *G*). Some corresponding features such as rings and straight-edged stripes are indicated by arrows. The periphery-to-area ratio (Fig. 5) showed little significant change between 10° and 40°C. At 40°C the 4.2-Å diffraction ring was no longer observable and the diffraction contrast micrograph became featureless (Fig. 6*D*).

PS-DPPC AT A MOLAR RATIO (1:10) Since solidus domains in pure DPPC were

measured to several micrometers in width (24), it was suspected that the molar ratio of PS/DPPC may affect the size of the domains. The average domain width measured from diffraction-contrast micrographs of PS/DPPC (1:10) bilayers was indeed found to be larger than those from PS/DPPC (1:2) at low temperatures. This is apparent from visual examination of the micrographs (Fig. 6*E*).

DISCUSSION

Although the existence of domains of different molecular packing is implied in the term "lateral phase separation," these domains have seldom been directly visualized and identified in terms of molecular packing in a lipid bilayer. In general, the domain features are beyond the resolution of light microscopes. The banded patterns associated with the P_β or $P_{\beta'}$ (40) phases have been used as a phase marker to identify domains on freeze-fracture faces by electron microscopy (27, 41). Because P phases exist only in some phospholipids and only within restricted temperature ranges, the application of this method to identify domains is limited. The repartitioning of integral proteins, as a result of membrane lipid phase separation, has also been used to indicate the geometry of lipid domains by electron microscopy (42–45). The average width of solidus domains may also be indirectly deduced from x-ray diffraction line-width measurement, and the area percentage of these domains from comparing integral intensities of the solidus and fluidus diffraction lines (40). Because of the difficulties involved in the latter method, quantitative comparison between microscopic measurements of domain area and macroscopically (by calorimetry, etc.) determined phase diagrams has not been given. With diffraction-contrast electron microscopy, the domains are visualized by utilizing the indigenous molecular packing phase to create domain contrast. Therefore, in principle, this method applies to any phase-separated system consisting of areas of different chain packings. Moreover, the observation is made at the actual temperature of the specimen; therefore, it is free of possible freezing artifacts. The micrographs represent a direct visual picture of domains of different molecular packing in lipid bilayers. The results of this study provided an independent proof that domains of different molecular packing did exist throughout the phase-separation range, and verified that the lower limit of domain size estimated by an x-ray diffraction experiment (40) was essentially correct.

Quantitative assessment of the domain geometry (Fig. 5) shows that in the DLPC/DPPC (1:1) mixture, there is an increase in the boundary length per area with temperature (a decrease in domain width). In the PS/DPPC (1:2) mixture, there seem to be no significant variations in domain width or in boundary length per unit area over the entire experimental temperature range. The values of boundary length per unit domain area remain $\sim 2\ \mu m^{-1}$. It should be noted that the domains observed in this experiment are areas of similar phase rather than areas of similar composition (23); their relationship depends on the miscibility of the system. Because the phase-transition temperature ranges of these two systems are approximately equal, the different geometrical phase behavior could be related to the following: (*a*) the DLPC/DPPC is a partially miscible system (25) whereas PS/DPPC is a completely miscible system (27); (*b*) bovine brain PS is a heterogeneous lipid; thus, the PS/DPPC mixtures is not strictly a binary system, and (*c*) PS/DPPC mixtures involve lipids of two different head groups. It is reasonable to argue that the less miscible DLPC/DPPC would tend to form large, stable single-component domains upon cooling, especially when the lower

melting point component is the pure DLPC rather than the heterogeneous PS. As a completely miscible system, PS/DPPC forms a solid solution upon cooling. The solidus domains of this mixture are expected to remain as smaller crystallites due to their heterogeneous composition. Cycling through the transition temperature range does not seem to have any significant effect on the domain geometry. The compositional heterogeneity seems to render the annealing (8) and repartitioning (7) processes less effective. It is interesting to note that PS/DPPC (1:10) mixture has larger solidus domains than PS/DPPC (1:2) at low temperatures (Fig. 6*E*). In the composition of (1:10), pure DPPC domains tend to crystallize out upon cooling, according to the phase diagram (27). The results suggest that homogeneous and immiscible systems tend to favor larger and less invaginated solidus domains.

Although it was not the primary aim of this microscopic study to provide an alternative way to measure macroscopic ratios of solidus and liquidus areas, the area ratio obtained from this study on planar single bilayers nevertheless followed in general those derived from calorimetric (25, 27) and freeze-fracture measurements on multilamellar vesicles (Fig. 4). In DLPC/DPPC mixtures, at temperatures around 10°C, the area percentage curve deduced from the phase diagram (reference 25, Fig. 5) is hypothetical since the theoretical solid phase line in that phase diagram is drawn without associated calorimetric data. When comparing analogous phase diagrams of DSPC/DMPC in reference 25, Fig. 4 with that from reference 20, Fig. 3B, the corresponding portion of the theoretical solid-phase line of the former deviates from the calorimetric data of the latter. Applying a similar correction to the hypothetical DPPC/DLPC solid-phase line (reference 25, Fig. 5) would put the percent line in Fig. 3 almost exactly over the microscope data points. In PS/DPPC mixtures, matching between diffraction-contrast measurements and predicted values is mostly within experimental error. The agreements show that the phase-separation ranges in single planar bilayers and in multilamellar vesicles are approximately the same. Similar agreement in the phase transition of a single component bilayer and the corresponding multilamellar vesicles has been shown (28). However, since the $P_{\beta'}$ phase is not known to exist in planar single bilayers (38), the phase diagrams of single bilayers and corresponding multilamellar vesicles may not be identical. Moreover, the wide-angle diffraction patterns in this experiment show no characteristics of acyl chain tilting (38). It seems that the solidus phase in these planar single bilayers is in the L_β or P_β phase rather than in the $P_{\beta'}$ phase. Because there is no thickness variation in a P_β-phase bilayer when viewed normal to the bilayer plane, its image is indistinguishable from that of an L-phase bilayer. The geometric parameters nevertheless show that the average area, the size and the shapes of solidus phase domains in multilamellar vesicles, and in planar bilayer are very similar, in spite of their possible differences in acyl chain tilting.

The limitations of the diffraction-contrast technique in this study are imposed by the low contrast and by radiation damage. These two parameters are related by the Rose equation (32). The threshold damage dose in this experiment is approximately equivalent to those in other low-dose electron microscopy experiments (32, 34). At a magnification of ×4,000, and with a beam dose of 5×10^{-5} coulomb/cm^2, electron images of molecular bilayers can be recorded above the statistic noise. With the same beam dose but at ten times the magnification, the image would have been below the noise level (34). Since the domains we intend to observe were expected to be about several tens of nanometers wide, using a lower magnification was justified. On the other hand, the contrast limitation in diffraction-contrast imaging is

given by the ratio of the diffraction to the background intensities passing through the filter openings. The percentage contrast is defined by $(I_{specific} - I_{background})/I_{background}$. The background intensity comes from inelastic and incoherent scattering. The contrast measured from densitometer tracings of the filtered diffraction patterns was ~35%. The percentage might be improved somewhat by narrowing the gap of the selection filter, but the high background rendered it impossible to exceed 50% contrast. An overlapping of the 4.2- and 4.7-Å diffraction lines reduces the contrast by another 20%. At temperatures near the upper limit of the phase-separation range, domain motion (39) further reduced the contrast. The limitations in diffraction contrast and in incident electron beam intensity pose an inherent physical barrier to improving the quality of diffraction-contrast images of lipid bilayers. However, information should still be retrievable up to a magnification of ×10,000.

The diffraction-contrast micrographs obtained in this study have shown the existence and provided primary geometrical data of domains of different molecular packings in single bilayers of mixed phospholipids through the phase-separation range. The sizes and shapes of these domains were found to depend on the miscibility and the chemical heterogeneity of their constituents. The geometric parameters obtained from this experiment should help in understanding many macroscopic measurements of bilayer properties believed to be related to microscopic structural discontinuities and defects. The application of this method to the study of more complex structures depends on improving contrast and resolution, as well as on the successful adaptation of various planar membrane formation techniques (46).

The helpful discussions and assistance of Drs. D. Papahadjopoulos, R. Pearson, and T. P. Stewart are appreciated.

The work was supported in part by grants BC-248 from the American Cancer Society and GM28120 from National Institutes of Health (NIH). The author is a recipient of a Career Development Award CA 00084 from the National Cancer Institute.

REFERENCES

1. Linden, C. D., K. L. Wright, H. M. McConnell, and C. F. Fox. 1973. Lateral phase separations in membrane lipids and the mechanism of sugar transport in *Escherichia coli*. *Proc. Natl. Acad. Sci. U. S. A.* 70:2271–2275.
2. Overath, P., M. Brenner, T. Gulik-Krzywicki, E. Shechter, L. Letellier. 1975. Lipid phase transitions in cytoplasmic and outer membranes of *Escherichia coli*. *Biochim. Biophys. Acta.* 389:358–369.
3. Verkleij, A. J., P. H. J. Vergergaert, L. L.M. Van Deenen, and P. F. Elberts. 1972. Phase transitions of phospholipid bilayers and membranes of acholeplasma laidlawii B visualized by freeze fracturing electron microscopy. *Biochim. Biophys. Acta.* 288:326–332.
4. Hochli, M. and C. R. Hackenbrock. 1976. Fluidity in mitochondrial membranes: thermotropic lateral translational motion of intramembrane particles. *Proc. Natl. Acad. Sci. U. S. A.* 73:1636–1640.
5. Melchior, D. L., and J. M. Steim. 1976. Thermotropic transitions in biomembranes. *Annu. Rev. Biophys. Bioeng.* 5:205–238.
6. Phillips, M. C., B. D. Ladbrooke, and D. Chapman. 1970. Molecular interactions in mixed lecithin systems. *Biochim. Biophys. Acta.* 196:35–44.
7. Lee, A. G. 1977. Lipid phase transitions and phase diagrams I. Lipid phase transitions. *Biochim. Biophys. Acta.* 472:237–281.
8. Lawaczeck, R., M. Kainosho, S. I. Chan. 1976. The formation and annealing of structural defects in lipid bilayer vesicles. *Biochim. Biophys. Acta.* 443:313–330.
9. Marsh, D., A. Watts, and P. F. Knowles. 1977. Cooperativity of the phase transition in single and multibilayer lipid vesicles. *Biochim. Biophys. Acta.* 465:500–514.
10. Papahadjopoulos, D., K. Jacobson, S. Nir, and T. Isac. 1973. Fluorescence polarization and permeability measurements concerning the effects of temperature and cholesterol. *Biochim. Biophys. Acta.* 311:330–348.

11. Blok, M.C., E. C. M. Van Der Neut-Kok, L. L. M. Van Deenen, and J. De Gier, 1975. The effect of chain length and lipid phase transition on the selective permeability properties of liposomes. *Biochim. Biophys. Acta.* 406:187–196.
12. W. T. Wickner. 1977. Role of hydrophobic forces in membrane protein asymmetry. *Biochemistry.* 16:254–258.
13. Pownall, H. J., J. B. Massey, S. K. Kusserow, and A. M. Gotto. 1979. Kinetics of lipid-protein interactions: effect of cholesterol on the association of human plasma high-density apolipoprotein A-I with L-α-dimyristoylphosphatidylcholine. *Biochemistry.* 18:574–579.
14. Wilschut, J. C., J. Regts, H. Westenberg, and G. Scherphof. 1978. Action of phospholipase A_2 on phosphatidylcholine bilayers. Effects of the phase transition, bilayer curvature and structural defects. *Biochim. Biophys. Acta.* 508:185–196.
15. Bretscher, M. S. 1976. Directed lipid flow in cell membranes. *Nature (Lond.).* 260:21–23.
16. Zagyansky, Y. A., and S. Jard. 1979. Does lectin-receptor complex formation produce zones of restricted mobility within the membrane? *Nature (Lond.).* 280:591–594.
17. Zakai, N., R. G. Kulka, and A. Loyter. 1977. Membrane ultrastructural changes during calcium phosphate-induced fusion of human erythrocyte ghosts. *Proc. Natl. Acad. Sci. U. S. A.* 74:2417–2421.
18. Cullis, P. R., and M. J. Hope. 1978. Effects of fusogenic agent on membrane structure of erythrocyte ghosts and the mechanism of membrane fusion. *Nature (Lond.).* 271:672–674.
19. Klausner, R. D., D. K. Bhalla, P. Dragsten, R. L. Hoover, and M. J. Karnovsky. 1980. Model for capping derived from inhibition of surface receptor capping by free fatty acids. *Proc. Natl. Acad. Sci. U. S. A.* 77:437-41.
20. Mabrey, S., and J. M. Sturtevant. 1976. Investigation of phase transitions of lipids and lipid mixtures by high sensitivity differential scanning calorimetry. *Proc. Natl. Acad. Sci. U. S. A.* 73:3862–66.
21. Freire, E., and R. Biltonen. 1978. Estimation of molecular averages and equilibrium fluctuations in lipid bilayer systems from the excess heat capacity function. *Biochim. Biophys. Acta.* 514:54–68.
22. Marcelja, S., and J. Wolfe. 1979. Properties of bilayer membranes in the phase transition or phase separation region. *Biochim. Biophys. Acta.* 557:24–31.
23. Freire, E., and B. Snyder. 1980. Estimation of the lateral distribution of molecules in two-component lipid bilayers. *Biochemistry.* 19:88–94.
24. Hui, S. W., and D. F. Parsons. 1975. Direct observation of domains in wet lipid bilayers. *Science (Wash., D.C.)* 190:383–4.
25. Van Dijck, P. W. M., A. J. Kaper, H. A. J. Oonk, and J. De Gier. 1977. Miscibility properties of binary phosphatidylcholine mixtures. *Biochim. Biophys. Acta.* 470:58–69.
26. de Kruyff, B., P. W. M. Van Dijck, R. A. Demell, A. Schuijff, F. Brants, and L. L. M. Van Deenen. 1974. Non-random distribution of cholesterol in phosphatidylcholine bilayers. *Biochim. Biophys. Acta.* 356:1–7.
27. Stewart, T. P., S. W. Hui, A. R. Portis, and D. Papahadjopoulos. 1979. Complex phase mixing of phosphatidylcholine and phosphatidylserine in multilamellar membrane vesicles. *Biochim. Biophys. Acta.* 556:1–16.
28. Hui, S. W., M. Cowden, D. F. Parsons, and D. Papahadjopoulos. 1975. Electron diffraction study of hydrated phospholipid single bilayers. Effects of temperature, hydration and surface pressure of the "precursor" monolayer. *Biochim. Biophys. Acta.* 382:265–275.
29. Hui, S. W., D. F. Parsons, and M. Cowden. 1974. Electron diffraction of wet phospholipid bilayers. *Proc. Natl. Acad. Sci.* U. S. A. 71:5068–5072.
30. Hui, S. W., G. G. Hausner, and D. F. Parsons. 1976. A temperature controlled hydration or environmental stage for the Siemens Elmiskop 1A. *J. Phys. Sci. Instrum.* 9:69–72.
31. Costello, M. J., and J. M. Corless. 1978. The direct measurement of temperature changes within freeze-fracture specimens during rapid quenching in liquid coolants. *J. Microsc.* 112:17–37.
32. Glaeser, R. M. 1975. Physical Aspects of Electron Microscopy and Microanalysis. Siegel and Beaman, editors. John Wiley and Sons, Inc., New York. 205–203.
33. Hui, S. W. 1977. Electron diffraction studies of membranes. *Biochim. Biophys. Acta.* 472:345–371.
34. Unwin, N., and R. Henderson. 1977. Molecular structure determination by electron microscopy of unstained crystalline specimens. *J. Mol. Biol.* 94:425–440.
35. Vainshtein, B. K. 1964. Structural Analysis by Electron Diffraction. Macmillan, Inc., New York 157–167.
36. Hall, C. E. 1966. Introduction to Electron Microscopy. McGraw-Hill, New York. 210.
37. Levine, Y. K. 1973. X-ray diffraction studies of membranes. Prog. Surf. Membr. Sci. 3:279–352.
38. Hui, S. W. 1976. The tilting of the hydrocarbon chains in a single bilayer of phospholipid. *Chem. Phys. Lipids.* 16:9–18.
39. Hui, S. W. 1976. Direct measurement of membrane motion and fluidity by electron microscopy. *Nature (Lond.).* 262:303–305.
40. Ranck, J. L., L. Mateu, D. M. Sadler, A. Tardieu, T. Gulik-Krzywicki, and V. Luzzati. 1974. Order-disorder conformational transitions of the hydrocarbon chains of lipids. *J. Mol. Biol.* 85:249–77.

41. C. W. M. Grant, S. Hong-Wei Wu, and H. McConnell. 1974. Lateral phase separations in binary lipid mixtures: correlation between spin label and freeze-fracture electron microscopic studies. *Biochim. Biophys. Acta.* 363:151–158.
42. Speth, V. and F. Wunderlich. 1973. Membranes of *Tetrahymena*. II. Direct visualization of reversible transitions in biomembranes' structure induced by temperature. *Biochim. Biophys. Acta.* 291:621–628.
43. Wallace, B. A., F. M. Richards, and D. M. Engleman. 1976. The influence of lipid state on the planar distribution of membrane proteins in *Acholeplasma laidlawii*. *J. Mol. Biol.* 107:255–269.
44. Kleemann W., and H. M. McConnell. 1976. Interactions of proteins and cholecterol with lipids in bilayer membranes. *Biochim. Biophys. Acta.* 419:206–222.
45. Hui, S. W., C. M. Stewart, M. P. Carpenter, and T. P. Stewart. 1980. Effects of cholesterol on lipid organization in human erythrocyte membrane. *J. Cell Biol.* 85:283–291.
46. Pattus, F., M. C. T. Piovant, C. J. Lazdunski, P. Desnuelle, and R. Verger. 1978. Spreading of biomembranes at the air-water interface. *Biochim. Biophys. Acta.* 507:71–82.